# Representing Equations of State With Strong First-Order Phase Transitions

Lee Lindblom,[1] Steve M. Lewis, and Fridolin Weber[1,2]

[1]*Department of Physics, University of California at San Diego, San Diego, California, 92093 USA*
[2]*Department of Physics, San Diego State University, San Diego, California, 92182 USA*

(Dated: March 27, 2025)

Parametric representations of the high-density nuclear equation of state are used in constructing models for interpreting the astrophysical observations of neutron stars. This study explores how accurately equations of state with strong first-order phase transitions can be represented using spectral or piecewise analytic methods that assume no *a priori* knowledge of the location or the strength of the phase transition. The model equations of state used in this study have phase transitions strong enough to induce a gravitational instability that terminates the sequence of stable neutron stars. These equations of state also admit a second sequence of stable stars with core matter that has undergone this strong first-order phase transition (possibly driven by quark deconfinement). These results indicate that spectral representations generally achieve somewhat higher accuracy than piecewise analytic representations having the same number of parameters. Both types of representation show power-law convergence at approximately the same rate.

## I. INTRODUCTION

Parametric representations of the nuclear equation of state are used in the construction of models designed to describe, and to understand at a deeper level, the astrophysical observations of neutron stars. For example, these representations can be used to solve the relativistic inverse stellar structure problem in which the equation of state of the stellar matter is determined from a knowledge of the star's macroscopic properties (e.g. their masses and radii) [1–4]. This inverse structure problem can be solved by adjusting the equation of state parameters to minimize the differences between the neutron-star observations and the models of those observed properties constructed from the equation of state representation.

The quantity and quality of the astrophysical observations of neutron stars has improved significantly over the past decade. The masses and radii of neutron stars have now been measured at the few percent level for dozens of neutron stars from observations of binary systems. Both mass and radius have been measured for a few individual neutron stars at the 10-20% level using x-ray observations [5–13]. And both mass and tidal deformability have also been measured using gravitational wave observations of binary merger events [14–16], presently at somewhat lower accuracy than that achieved by the best x-ray observations.

Reliable parametric representations of the high density neutron-star equation of state are needed to construct useful models of these observations. These representations must be capable of representing the large class of possible neutron-star equations of state at an accuracy level sufficient for the current observations. And these representations should be flexible enough to accommodate more accurate future observations as they become available. A number of such representations have been proposed, for example see Refs. [17–22]. Some of these use spectral methods to represent the equation of state over the full range of pressures expected in neutron-star cores, while others use piecewise analytic representations on a collection of shorter pressure intervals that together span the range of core pressures. Both types of representations have been shown to be convergent (in the sense that their accuracies can be increased simply by increasing the number of parameters) for a large collection of nuclear-theory based equations of state [19], including examples with a wide range of phase transitions [22, 23]. These representations have also been shown to be accurate enough to allow solutions of the relativistic inverse structure problem with accuracies commensurate with the accuracy of the available data from neutron-star observations [24].

Spectral methods provide the most efficient representations of smooth equations of state, converging exponentially as the number $N$ of spectral basis functions is increased (i.e. with errors decreasing faster than any power of $1/N$). In comparison, piecewise analytic representations typically have power-law convergence (i.e. with errors decreasing as $1/N^k$ for some particular $k$). It is less widely appreciated that spectral representations of non-smooth functions (e.g. equations of state with first- or second-order phase transitions) are still convergent, but with power-law rather than exponential convergence rates [25].

Tests of representations of neutron-star equations of state with phase transitions of various sizes [22, 23] showed that even for these cases, the spectral representations were generally more accurate than the piecewise analytic representations having the same number of adjustable parameters. The sizes of the first-order phase transitions included in those studies were limited to discontinuities small enough that they could occur within the contiguous family of neutron stars. Sufficiently strong first-order phase transitions trigger an instability that terminates the sequence of stable neutron stars [26]. Representations of the first-order phase transition that first triggers this instability were studied in Refs. [22, 23], but representations of stronger first-order phase transitions have not yet been studied.

There has been some interest recently in the possibil-

ity that strong phase transitions could in some cases lead to a disconnected sequence of stable higher density relativistic stars [20, 27, 28]. The accuracy and convergence properties of spectral representations of such equations of state have not been determined at this time. The purpose of this study is to perform those tests and to evaluate the relative efficiencies of spectral and piecewise analytic representations of equations of state with these strong phase transitions. The model equations of state used in this study include phase transitions intended to describe the possible transition from hadron to quark matter [27]. These phase transitions are strong enough to terminate the contiguous sequence of neutron stars, and they allow a second disconnected sequence of stable relativistic stars with quark matter cores.

Section II describes in detail the model equations of state used in this study. These equations of state are based on the ACB4 and ACB5 models of hadron-quark phase transitions introduced in Ref. [27]. The versions of these equations of state used in this study are those adapted in Ref. [29] using a multi-polytrope representation with a Maxwell construction. This study also considers the generalizations introduced in Ref. [29], which incorporate a mixed-phase region at the hadron-quark interface, mimicking finite-size effects associated with a "pasta" phase [30, 31].

The equation of state representations used in this study are a causal Chebyshev polynomial based spectral representation [22], and a causal piecewise analytic representation [19]. These representations are described in Secs. III A and III B respectively. They are used to construct model equations of state that cover the full range of pressures that exist in the cores of both neutron and quark stars. Section III C introduces two-zone equation of state representations. These composite representations split the pressure range at the phase transition point with separate spectral (or piecewise analytic) representations below and above this point. These above and below representations are then combined to form a composite representation which includes three additional parameters that determine the location and size of the phase transition point.

Section IV of this study describes how the optimal representations of the hadron-quark equations of state are constructed for this study. Section V describes the numerical accuracy and convergence results obtained for the model equations of state with hadron-quark phase transitions described in Sec. II, using the various representation methods described in Sec. III. These results are discussed in Sec. VI. They show that the accuracy and convergence rates of the spectral and the piecewise analytic representations are comparable, with the spectral representations generally being somewhat more accurate than the piecewise analytic representations having the same number of adjustable parameters. The two zone representations are expected to become more accurate than their one zone counterparts in the limit of large parameter numbers. However the tests performed in this study using eleven or fewer parameters show that the one zone spectral and piecewise analytic representations are more accurate than their two zone counterparts with the same number of parameters.

## II. MODEL EQUATIONS OF STATE

The model equations of state used in this study describe possible strong hadron-quark phase transitions in neutron-star matter. This study uses the ACB4 and ACB5 equations of state introduced in Ref. [27]. These equations of state feature first-order phase transitions, which induce gravitational instabilities leading to the termination of the stable hadronic neutron star sequence at approximately $2.0M_\odot$ for ACB4 and $1.4M_\odot$ for ACB5. These equations of state also admit a disconnected branch of stable hybrid stars whose cores consist of the higher density quark matter. The ACB4 ($\Delta_{\rm P}$) and ACB5 ($\Delta_{\rm P}$) equations of state introduced in Ref. [29] are generalizations of ACB4 and ACB5 that use second-order phase transitions to model a mixed phase region where the transition from hadron to quark matter takes place over a range of pressures determined by the parameter $\Delta_{\rm P}$. These smoother transitions are designed to mimic "pasta" structures in which hadron and quark matter coexist at the same pressure, see Refs. [30–32]. The parameter value $\Delta_{\rm P} = 0$ corresponds to the original ACB4 and ACB5 equations of state with first-order phase transitions, while the larger $\Delta_{\rm P}$ values describe smoother more gradual second-order transitions between the hadron and quark phases.

Figures 1 and 2 illustrate the ACB4($\Delta_{\rm P}$) and ACB5($\Delta_{\rm P}$) equations of state over the range of pressures used in this study to evaluate the accuracy of spectral and piecewise analytic representations. The lower end of this range, $p_{\rm min} = 1.23592430\times10^{32}$ erg/cm$^3$, was chosen to correspond to the density, $\epsilon_{\rm min} = 5.41165156 \times 10^{13}$ g/cm$^3$, which is about one fifth normal nuclear density. The upper end of the pressure range, $p_{\rm max} = 1.13139676 \times 10^{36}$ erg/cm$^3$, corresponds to the central pressures of the maximum mass quark stars that can be constructed from the ACB4($\Delta_{\rm P}$) equations of state. Figures 3 and 4 illustrate in more detail the regions of the ACB4($\Delta_{\rm P}$) and ACB5($\Delta_{\rm P}$) equations of state where the phase transitions occur.

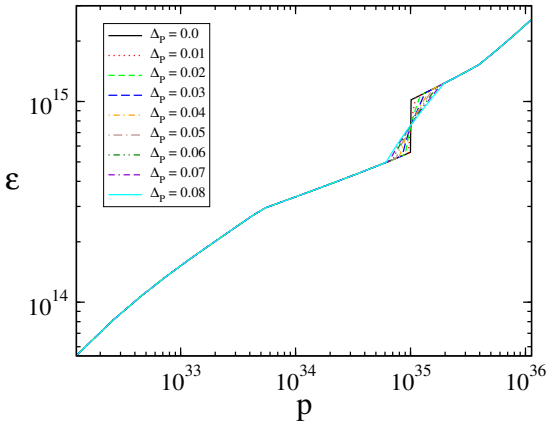


FIG. 1: This figure illustrates the ACB4($\Delta_P$) equations of state that have strong hadron-quark phase transitions at the central pressure of a 2.0 $M_\odot$ neutron star model. The total energy density $\epsilon$ and pressure $p$ are expressed in cgs units: g/cm$^3$ and erg/cm$^3$ respectively. The parameter $\Delta_P$ determines the width of the pressure region over which the phase transitions occur.

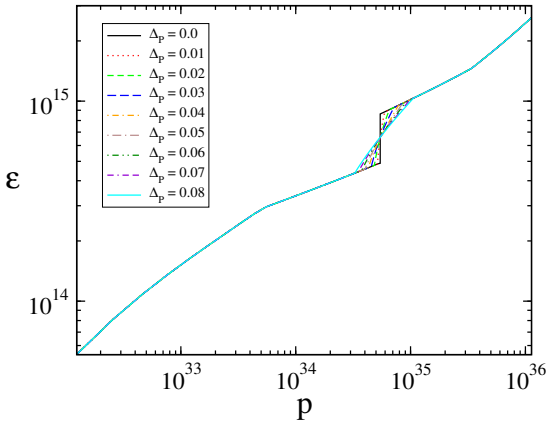


FIG. 2: This figure illustrates the ACB5($\Delta_P$) equations of state that have strong hadron-quark phase transitions at the central pressure of a 1.4 $M_\odot$ neutron star model. The total energy density $\epsilon$ and pressure $p$ are expressed in cgs units: g/cm$^3$ and erg/cm$^3$ respectively. The parameter $\Delta_P$ determines the width of the pressure region over which the phase transitions occur.

Figures 5 and 6 illustrate the mass-radius curves obtained by solving the Oppenheimer-Volkoff relativistic stellar structure equations [33] using the ACB4($\Delta_P$) and ACB5($\Delta_P$) equations of state respectively. The stellar models lying between the maxima and the subsequent minima of some of these mass-radius curves are unstable to a general relativistic gravitational instability that triggers collapse to a black hole. The curves in Fig. 5 show that the ACB4($\Delta_P$) equations of state with $\Delta_P < 0.05$ have maxima that trigger this instability, while also admitting stable composite hadron-quark stars with larger central densities. Similarly the curves in Fig. 6 show that the ACB5($\Delta_P$) equations of state with $\Delta_P < 0.02$

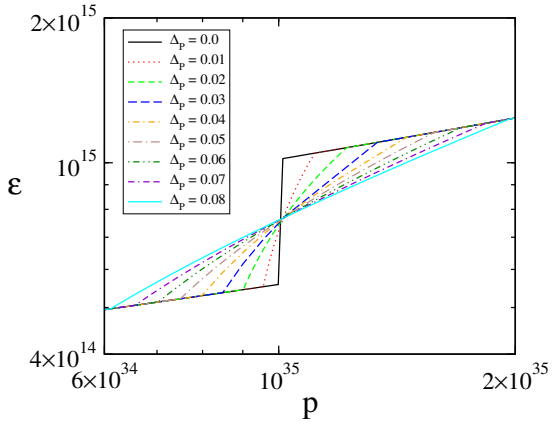


FIG. 3: This figure illustrates in more detail the regions of the ACB4($\Delta_P$) equations of state where the strong hadron-quark phase transitions occur. The total energy density $\epsilon$ and pressure $p$ are expressed in cgs units: g/cm$^3$ and erg/cm$^3$ respectively. The parameter $\Delta_P$ determines the width of the pressure region over which the phase transitions occur.

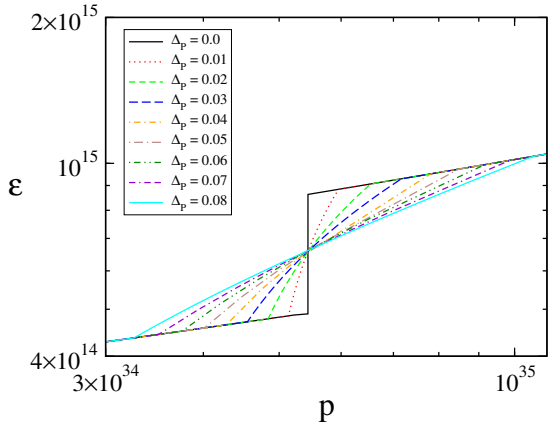


FIG. 4: This figure illustrates in more detail the regions of the ACB5($\Delta_P$) equations of state where the strong hadron-quark phase transitions occur. The total energy density $\epsilon$ and pressure $p$ are expressed in cgs units: g/cm$^3$ and erg/cm$^3$ respectively. The parameter $\Delta_P$ determines the width of the pressure region over which the phase transitions occur.

trigger this instability, while also admitting stable composite hadron-quark stars with larger central densities. The maximum masses and central pressures of the stable composite hadron-quark stars obtained using either the ACB4($\Delta_P$) or the ACB5($\Delta_P$) equations of state are very insensitive to the width of the phase transition region determined by the parameter $\Delta_P$.

## III. CAUSAL PARAMETRIC EQUATION OF STATE REPRESENTATIONS

This section describes the general methods used to construct the causal parametric representations of the high-density neutron-star equations of state used in this study.

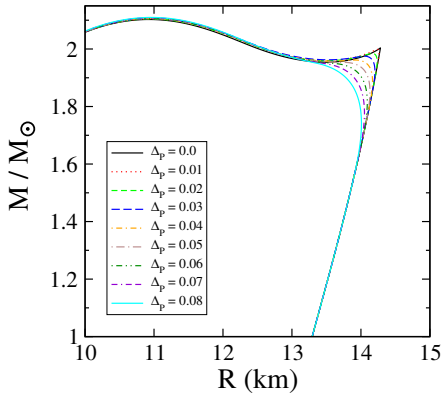


FIG. 5: This figure illustrates the mass-radius curves obtained by solving the Oppenheimer-Volkoff relativistic stellar structure equations using the ACB4($\Delta_{\rm P}$) equations of state.

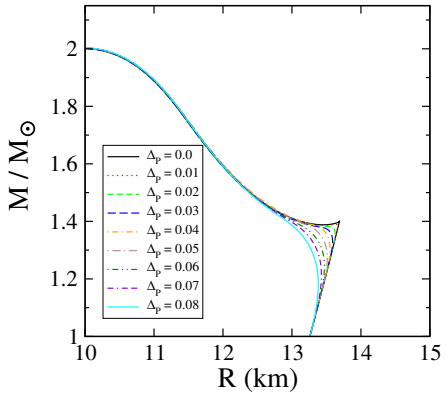


FIG. 6: This figure illustrates the mass-radius curves obtained by solving the Oppenheimer-Volkoff relativistic stellar structure equations using the ACB5($\Delta_{\rm P}$) equations of state.

These methods are applied in Secs. III A and III B to construct the particular spectral and the piecewise analytic representations used here. Section III C introduces two zone equation of state representations that split the pressure range at the phase transition point, with separate spectral (or piecewise analytic) representations below and above this point.

The speed of sound, $v$, in a relativistic barotropic fluid is determined by the equation of state: $v^2 = dp/d\epsilon$ [34]. These sound speeds satisfy the thermodynamic stability condition, $v^2 \geq 0$, and causality condition, $v^2 \leq c^2$ (where $c$ is the speed of light), if and only if the velocity function $\Upsilon$,

$$\Upsilon = \frac{c^2 - v^2}{v^2}, \tag{1}$$

is non-negative, $\Upsilon \geq 0$.

The velocity function $\Upsilon$ is determined by the equation of state: $\Upsilon(p) = c^2\, d\epsilon/dp - 1$. Conversely, $\Upsilon(p)$ can be used as a generating function from which the standard equation of state, $\epsilon = \epsilon(p)$, can be determined by quadrature. The definition of the velocity function $\Upsilon(p)$ can be re-written as the ordinary differential equation,

$$\frac{d\epsilon(p)}{dp} = \frac{1}{c^2} + \frac{\Upsilon(p)}{c^2}. \tag{2}$$

which can then be integrated to determine the equation of state, $\epsilon = \epsilon(p)$:

$$\epsilon(p) = \epsilon_{\rm min} + \frac{p - p_{\rm min}}{c^2} + \frac{1}{c^2}\int_{p_{\rm min}}^{p} \Upsilon(p')dp'. \tag{3}$$

The velocity functions $\Upsilon(p, \upsilon_a)$ used in this study depend on a series of parameters $\upsilon_a$, for $1 \leq a \leq N_{\rm parms}$. Equation (3) therefore determines a family of equations of state, $\epsilon = \epsilon(p, \upsilon_a)$, whose parameters can be adjusted to model realistic physical equations of state.

The process of finding the optimal choice of parameters needed to fit a particular equation of state generally requires a knowledge of how the parametric equation of state, $\epsilon(p, \upsilon_a)$, changes as the parameters, $\upsilon_a$, are varied. In some cases the most efficient way to determine $\partial\epsilon(p, \upsilon_b)/\partial\upsilon_a$ is to evaluate the integrals,

$$\frac{\partial\epsilon(p, \upsilon_b)}{\partial\upsilon_a} = \frac{1}{c^2}\int_{p_{\rm min}}^{p} \frac{\partial\Upsilon(p', \upsilon_b)}{\partial\upsilon_a}dp'. \tag{4}$$

In more complicated cases it may be more efficient to evaluate these derivatives numerically using finite difference expressions, e.g.,

$$\frac{\partial\epsilon(p, \upsilon_a)}{\partial\upsilon_a} = \frac{\epsilon(p, \upsilon_a + \delta\upsilon_a) - \epsilon(p, \upsilon_a - \delta\upsilon_a)}{2\delta\upsilon_a} + \mathcal{O}(\delta\upsilon_a^2). \tag{5}$$

### A. Spectral Representations

Causal parametric representations of the neutron-star equation of state can be constructed by expressing the velocity function, $\Upsilon(p, \upsilon_a)$, as a spectral expansion based on Chebyshev polynomials (see Ref. [22]):

$$\Upsilon(p, \upsilon_a) = \Upsilon_{\rm min} \exp\left\{\sum_{a=0}^{N_{\rm parms}-1} \upsilon_a(1+y)T_a(y)\right\}, \tag{6}$$

where the $T_a(y)$ are Chebyshev polynomials. The variable $y$ (defined below) is a function of the pressure having the property that $y = -1$ when $p = p_{\rm min}$. The constant $\Upsilon_{\rm min}$ is evaluated from the low-density equation of state at the point $p = p_{\rm min}$ where it matches onto the high density spectral representation determined by Eq. (6). Choosing $\Upsilon_{\rm min}$ in this way ensures that no artificial second-order phase-transition discontinuity is introduced at the matching point. These expansions guarantee that $\Upsilon(p) \geq 0$ for every choice of $\upsilon_a$. Therefore any equation of state determined from one of these $\Upsilon(p, \upsilon_a)$ automatically satisfies the causality and thermodynamic stability conditions.

Chebyshev polynomials are defined by the recursion relation $T_{a+1}(y) = 2yT_a(y) - T_{a-1}(y)$ with $T_0(y) = 1$ and $T_1(y) = y$. Spectral expansions using Chebyshev basis functions are well behaved on the domain $-1 \leq y \leq 1$ [25]. The variable $y$ used here has been chosen to be the following linear function of $\log p$,

$$y(p) = -1 + 2\log\left(\frac{p}{p_{\rm min}}\right)\left[\log\left(\frac{p_{\rm max}}{p_{\rm min}}\right)\right]^{-1}, \quad (7)$$

to ensure that $-1 \leq y \leq 1$ for pressures in the range $p_{\rm min} \leq p \leq p_{\rm max}$. The factor $1+y$ that appears in Eq. (6) ensures that $\Upsilon(p, \upsilon_a)$ has the limit, $\Upsilon(p_{\rm min}, \upsilon_a) = \Upsilon_{\rm min}$, for every choice of spectral parameters $\upsilon_a$. The partial derivatives $\partial\epsilon(p, \upsilon_b)/\partial\upsilon_a$ needed to evaluate the integrals in Eq. (4) for this spectral representation are given by:

$$\frac{\partial\Upsilon(p, \upsilon_b)}{\partial\upsilon_a} = [1 + y(p)]T_a[y(p)]\Upsilon(p, \upsilon_b). \quad (8)$$

### B. Piecewise Analytic Representations

Causal piecewise-analytical representations are constructed by subdividing the pressure domain $[p_{\rm min}, p_{\rm max}]$ into $N$ subdomains with $p_{\rm min} = p_0 < p_1 < ... < p_{N-1} < p_N = p_{\rm max}$ (see Ref. [19]). In this study the $p_k$ are chosen to be distributed logarithmically so that $p_k = p_{k-1}(p_{\rm max}/p_{\rm min})^{1/N}$ for each $k = 1, ..., N$. In these representations the velocity function $\Upsilon(p)$ is taken to be a simple power law of the pressure:

$$\Upsilon(p, \upsilon_k) = \Upsilon_k\left(\frac{p}{p_k}\right)^{\upsilon_{k+1}}, \quad (9)$$

in the subdomain $p_k \leq p \leq p_{k+1}$. The adjustable parameters $\Upsilon_k$ and $\upsilon_{k+1}$ determine its properties in each subdomain. The integral in Eq. (3) for this $\Upsilon(p)$ is easy to perform, resulting in the following expression for $\epsilon(p, \upsilon_k)$

$$\begin{aligned}\epsilon(p, \upsilon_k) &= \epsilon_k + \frac{p - p_k}{c^2} \\ &\quad + \frac{p_k\Upsilon_k}{(1+\upsilon_{k+1})c^2}\left[\left(\frac{p}{p_k}\right)^{1+\upsilon_{k+1}} - 1\right] \quad (10)\end{aligned}$$

in the pressure subdomain $p_k \leq p < p_{k+1}$.

The constants $\Upsilon_k$ and $\epsilon_k$ for the piecewise analytic representations studied here are determined iteratively by enforcing continuity of $\Upsilon(p)$ and $\epsilon(p)$ at the pressure subdomain boundaries:

$$\Upsilon_k = \Upsilon_{k-1}\left(\frac{p_k}{p_{k-1}}\right)^{\upsilon_k}, \quad (11)$$

$$\begin{aligned}\epsilon_k &= \epsilon_{k-1} + \frac{p_k - p_{k-1}}{c^2} \\ &\quad + \frac{p_{k-1}\Upsilon_{k-1}}{(1+\upsilon_k)c^2}\left[\left(\frac{p_k}{p_{k-1}}\right)^{1+\upsilon_k} - 1\right], \quad (12)\end{aligned}$$

with $\Upsilon_0 = \Upsilon_{\rm min}$. The remaining constants $\upsilon_k$ for $1 \leq k \leq N = N_{\rm parms}$ are the independent parameters that determine the equation of state in each pressure subdomain. The analytic expressions for the derivatives $\partial\epsilon(p, \upsilon_b)/\partial\upsilon_a$ are quite complicated for these representations, so these derivatives have been computed numerically for this study using Eq. (5).

### C. Two Zone Representations

The equation of state representations presented in Secs. III A and III B provide unified descriptions of the equation of state on the domain $p_{\rm min} \leq p \leq p_{\rm max}$. When there is a large phase transition at a pressure $p_{\rm pt}$ somewhere in this domain, $p_{\rm min} \leq p_{\rm pt} \leq p_{\rm max}$, it may be possible to construct more efficient representations by breaking the original domain into two separate zones with pressures below and above the phase transition point. This can be done by constructing a representation in the first zone, $p_{\rm min} \leq p \leq p_{\rm pt}$, as described in Sec. III A or III B using the additional parameter $p_{\rm pt}$ that determines the location of the phase transition. A separate representation can similarly be constructed in the second zone, $p_{\rm pt} \leq p \leq p_{\rm max}$, by introducing two additional parameters $\epsilon_{\rm pt}$ and $\Upsilon_{\rm pt}$ that describe the total energy density and the sound speed just above the phase transition boundary. The resulting two zone representation requires a total of $N_{\rm parms} = 3 + N^{<}_{\rm parms} + N^{>}_{\rm parms}$ parameters, where $N^{>}_{\rm parms}$ and $N^{<}_{\rm parms}$ are the number of parameters needed to specify the spectral or piecewise representations in the zones above and below the phase transition point.

## IV. CONSTRUCTING OPTIMAL PARAMETRIC REPRESENTATIONS

Each of the model equations of state used in this study, ACB4($\Delta_{\rm P}$) and ACB5($\Delta_{\rm P}$), consists of a table of energy-density pressure pairs: $\{\epsilon_i, p_i\}$ for $1 \leq i \leq N_{\rm eos}$. A parametric representation of one of these equations of state consists of a function $\epsilon(p, \upsilon_a)$ and the values of the parameters $\upsilon_a$ for $1 \leq a \leq N_{\rm parms}$ that determine the energy density as a function of the pressure. The accuracy of a particular representation is determined by evaluating the dimensionless error residual $\chi(\upsilon_a)$, defined by

$$\chi^2(\upsilon_a) = \sum_{i=1}^{N_{\rm eos}} \frac{1}{N_{\rm eos}}\left\{\log\left[\frac{\epsilon(p_i, \upsilon_a)}{\epsilon_i}\right]\right\}^2. \quad (13)$$

The optimal choice of the parameters $\upsilon_a$ to represent a particular equation of state $\{\epsilon_i, p_i\}$ is obtained by minimizing $\chi(\upsilon_a)$ with respect to variations in each of the parameters $\upsilon_a$. This minimization is carried out numerically in this study using the Levenberg-Marquardt method [35]. This minimization process requires a knowledge of the derivatives of $\chi^2(\upsilon_a)$ with respect to the pa-

rameters $\upsilon_a$. These derivatives are determined by the derivatives of $\epsilon(p, \upsilon_a)$,

$$\frac{\partial \chi^2}{\partial \upsilon_a} = \frac{2}{N_{\rm eos}} \sum_{i=1}^{N_{\rm eos}} \frac{\partial \log \epsilon(p_i, \upsilon_b)}{\partial \upsilon_a} \log \left[ \frac{\epsilon(p_i, \upsilon_b)}{\epsilon_i} \right], \quad (14)$$

which in turn are determined for this study using Eq. (4) or (5).

## V. NUMERICAL RESULTS

Causal spectral representations of the high-density portions of the ACB4($\Delta_{\rm P}$) and ACB5($\Delta_{\rm P}$) equations of state have been constructed numerically over a range of pressures, $p_{\rm min} \le p \le p_{\rm max}$, using the methods described in Secs. III A and IV. The lower end of the pressure range, $p_{\rm min} = 1.23592430 \times 10^{32}$ erg/cm$^3$, was chosen to be the point in the exact equation of state tables corresponding to the density, $\epsilon_{\rm min} = 5.41165156 \times 10^{13}$ g/cm$^3$, which is about one fifth normal nuclear density. The upper limit of this pressure range, $p_{\rm max} = 1.13139676 \times 10^{36}$ erg/cm$^3$, corresponds to the central pressures of the maximum mass quark stars that can be constructed from the ACB4($\Delta_{\rm P}$) equations of state. The value of the velocity parameter $\Upsilon_{\rm min} = 13.7751914$ was chosen to ensure that the spectral representations do not introduce a nonphysical second-order phase transition at the $p = p_{\rm min}$ point.

Figures 7 and 8 show the minimum values of the equation of state error measures, $\chi$ defined in Eq. (14), as functions of the number of spectral parameters, $N_{\rm parms}$, for the spectral representations of the ACB4($\Delta_{\rm P}$) and ACB5($\Delta_{\rm P}$) equations of state. These results show that the spectral representations of the equations of state with second-order phase transitions, i.e. those with $\Delta_{\rm P} > 0$, converge more rapidly than the representation of the discontinuous $\Delta_{\rm P} = 0$ equation of state. Nevertheless, the spectral representations of the $\Delta_{\rm P} = 0$ equations of state are convergent with $\chi$ decreasing monotonically from $\chi \approx 0.5$ for $N_{\rm parms} = 1$ to $\chi \approx 0.06$ for $N_{\rm parms} = 10$.

Piecewise analytic representations of the high-density portions of the ACB4($\Delta_{\rm P}$) and ACB5($\Delta_{\rm P}$) equations of state have also been constructed numerically using the methods described in Secs. III B and IV. The values of the equation of state parameters used for these representations cover the same pressure range as those used for the spectral representations: $p_0 = p_{\rm min} = 1.23592430 \times 10^{32}$ erg/cm$^3$, $p_{N_{\rm parms}} = p_{\rm max} = 1.13139676 \times 10^{36}$ erg/cm$^3$, $\epsilon_0 = \epsilon_{\rm min} = 5.41165156 \times 10^{13}$ g/cm$^3$, and $\Upsilon_0 = \Upsilon_{\rm min} = 13.7751914$.

Figures 9 and 10 show the minimum values of the equation of state error measure, $\chi$, defined in Eq. (14) as functions of the number of parameters, $N_{\rm parms}$, for the piecewise analytic fits to the ACB4($\Delta_{\rm P}$) and ACB5($\Delta_{\rm P}$) equations of state. Like the spectral representations, these

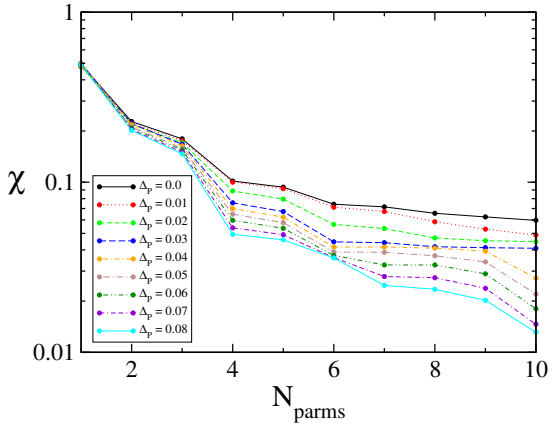


FIG. 7: This figure illustrates the equation of state error measures, $\chi$, as functions of the number of spectral parameters $N_{\rm parms}$ for the causal Chebyshev polynomial representations of the ACB4($\Delta_{\rm P}$) equations of state.

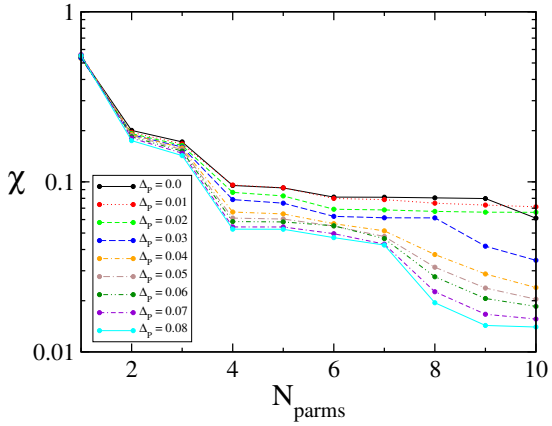


FIG. 8: This figure illustrates the equation of state error measures, $\chi$, as functions of the number of spectral parameters $N_{\rm parms}$ for the causal Chebyshev polynomial representations of the ACB5($\Delta_{\rm P}$) equations of state.

results show that the piecewise analytic representations of the smoother equations of state with $\Delta_{\rm P} > 0$ have smaller errors than than the representation of the discontinuous $\Delta_{\rm P} = 0$ equation of state, and that the values of $\chi$ generally get smaller as $N_{\rm parms}$ increases. Unlike the results for the spectral representations, however, the values of $\chi$ for these piecewise analytic representations are not strictly decreasing as $N_{\rm parms}$ increases. This nonmonotonic behavior appears to be caused by the changes in the proximity of the closest subdomain boundary to the phase transition point as $N_{\rm parms}$ is increased.

Figure 11 presents a direct comparison between the causal Chebyshev spectral representations of the discontinuous ACB4 and ACB5 equations of state with $\Delta_{\rm P} = 0$, and their causal piecewise analytic representations. These results show that the spectral and the piecewise analytic representations have comparable accuracies. The values of $\chi$ for the spectral representa-

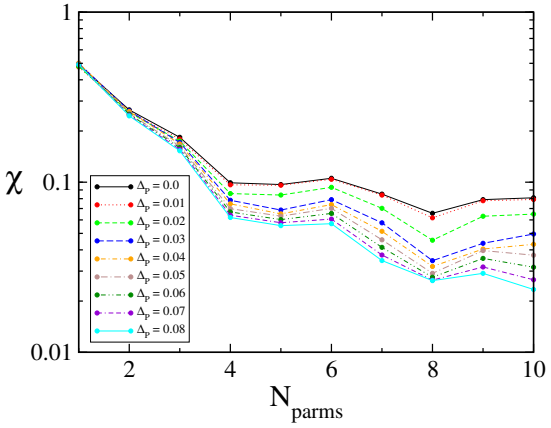


FIG. 9: This figure illustrates the equation of state error measures, $\chi$, as functions of the number of spectral parameters $N_{\rm parms}$ for the causal piecewise analytic representations of the ACB4($\Delta_{\rm P}$) equations of state.

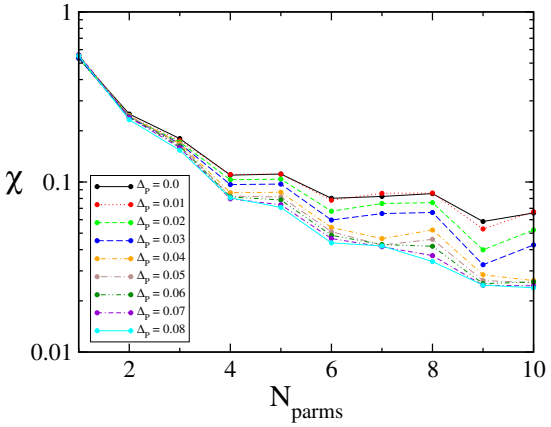


FIG. 10: This figure illustrates the equation of state error measures, $\chi$, as functions of the number of spectral parameters $N_{\rm parms}$ for the causal piecewise analytic representations of the ACB5($\Delta_{\rm P}$) equations of state.

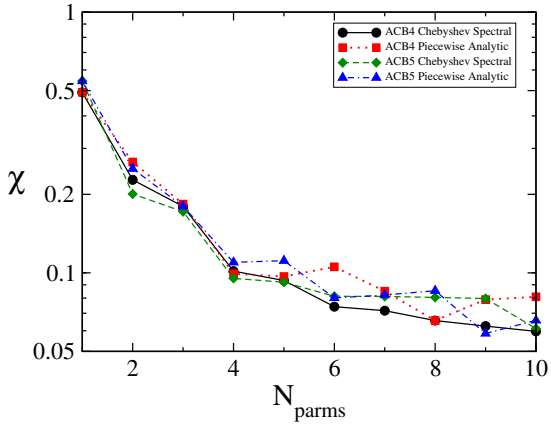


FIG. 11: This figure illustrates the error measures $\chi$ for the causal Chebyshev spectral and the causal piecewise analytic representations of the ACB4 and ACB5 equations of state with $\Delta_{\mathcal{P}} = 0$ as functions of the number of parameters $N_{\rm parms}$.

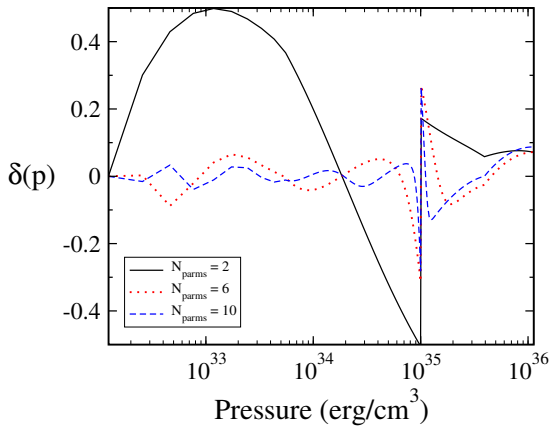


FIG. 12: This figure illustrates the fractional errors, $\delta(p) = 1 - \epsilon(p, \upsilon_a)/\epsilon_{\rm exact}(p)$, for the causal Chebyshev spectral representations of the ACB4($\Delta_{\rm P} = 0$) equation of state with $N_{\rm parms} = 2$, 6, or 10 spectral parameters.

tions are generally somewhat smaller than those for the piecewise analytic representations. Therefore the spectral representations are generally somewhat more accurate than the piecewise analytic representations with the same number of parameters.

Figures 12 and 13 illustrate the pointwise accuracies of the causal Chebyshev spectral and the causal piecewise analytic representations of the discontinuous ACB4 equation of state with $\Delta_{\rm P} = 0$. These figures show the pointwise fractional errors, $\delta(p)$, defined by,

$$\delta(p) = 1 - \frac{\epsilon(p, \upsilon_a)}{\epsilon_{\rm exact}(p)}. \tag{15}$$

For clarity in these figures, only the errors for the $N_{\rm parms} = 2$, 6, and 10 representations are shown. These figures illustrate that both the spectral and piecewise analytic representations make significant errors at and near the phase transition points, but that both types of representation become more accurate overall as the number of parameters is increased. The non-smooth features in these figures near the lower end of the pressure range are caused by the sparseness of the points in the exact ACB4 equation of state tables $\{\epsilon_i, p_i\}$ in that region.

The two zone spectral and piecewise analytic representations as described in Secs. III C and IV have also been constructed in this study for the discontinuous ACB4 equation of state with $\Delta_{\rm P} = 0$. The number of parameters in these two zone representations are the sum of the parameters needed in the two independent zones plus three additional parameters needed to describe the location and size of the phase transition point. Thus the total number of parameters is given by $N_{\rm parms} = 3 + N^{<}_{\rm parms} + N^{>}_{\rm parms}$, where $N^{>}_{\rm parms}$ and $N^{<}_{\rm parms}$ are the number of parameters needed to specify the spectral or piecewise analytic representations in the regions above

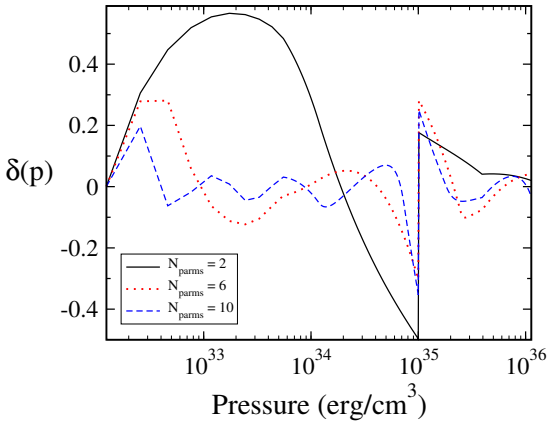


FIG. 13: This figure illustrates the fractional errors, $\delta(p) = 1 - \epsilon(p, \upsilon_a)/\epsilon_{\rm exact}(p)$, for the causal piecewise analytic representations of the ACB4($\Delta_{\rm P} = 0$) equation of state with $N_{\rm parms} = 2$, 6, or 10 parameters.

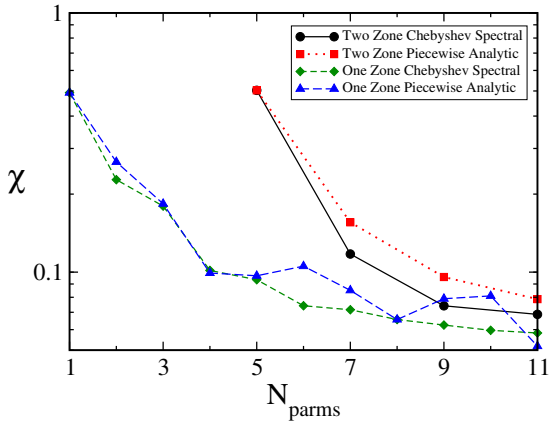


FIG. 14: This figure illustrates the equation of state accuracy measure $\chi$ as a function of $N_{\rm parms}$ for one and two zone representations of the ACB4($\Delta_{\rm P} = 0$) equation of state based on Chebyshev spectral or piecewise analytic methods. These results show that the one zone representations are more efficient than the two zone representations for $N_{\rm parms} \leq 11$.

and below the phase transition point. The values of the three additional parameters needed to specify the phase transition properties in this study have been set to the optimal values from the exact ACB4 equation of state: $p_{\rm pt} = 1.01221731 \times 10^{35}$, $\epsilon_{\rm pt} = 1.01995577 \times 10^{15}$ and $\Upsilon_{\rm pt} = 0.586578885$. Two zone representations have been computed for this study with $N^{<}_{\rm parms} = N^{>}_{\rm parms} = 1$, 2, 3, and 4, thus resulting in representations with $N_{\rm parms} = 5$, 7, 9, and 11. Figure 14 illustrates the relationships between the accuracies of the one and two zone spectral and piecewise analytic representations. This figure shows that the one zone representations are more accurate than the two zone representations for the range of models studied here: $N_{\rm parms} \leq 11$. This figure also shows that the spectral representations are generally more accurate than the piecewise analytic representations having the same number of parameters.

## VI. DISCUSSION

In summary, tests have been performed in this study to determine the accuracy and convergence rates of the spectral and the piecewise analytic representations of neutron-star equations of state with strong hadron-quark phase transitions. These results show that both types of representation are generally convergent as the number of parameters is increased. These representations have comparable accuracies, with the spectral representations generally being slightly more accurate than the piecewise analytic representations having the same number of adjustable parameters. The two zone spectral representations should converge exponentially, and should therefore become more accurate than their one zone counterparts in the limit of large parameter numbers. However the tests performed in this study using eleven or fewer parameters show that the one zone spectral and piecewise analytic representations are more accurate than their two zone counterparts with the same number of parameters. The analysis in Ref. [24] shows that very high accuracy observations of neutron-star masses and radii are needed before equation of state representations with large numbers of parameters will be useful in determining the equation of state more accurately. Therefore it is not likely that two zone neutron-star representations will be useful for observational data analysis in the near future.

Figure 11 shows that the causal Chebyshev spectral and the causal piecewise analytic representations of the discontinuous ACB4 and ACB5 equations of state with $\Delta_{\rm P} = 0$ have comparable accuracies. It is possible that other more accurate piecewise analytic representations

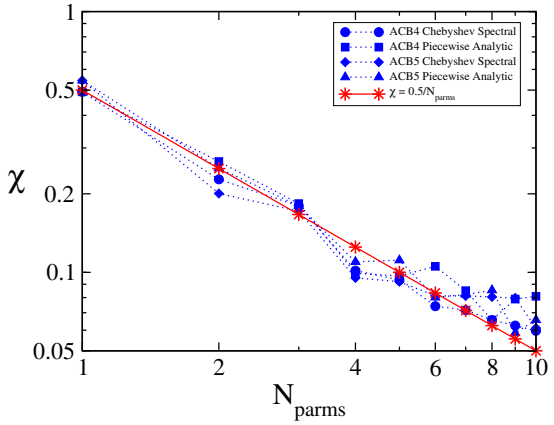


FIG. 15: This figure illustrates the convergence rates of the representations of the discontinuous ACB4 and ACB5 equations of state with $\Delta_{\rm P} = 0$. The (blue) dotted curves reproduce the data shown in Fig. 11, while the (red) solid curve is the function $\chi = 0.5/N_{\rm parms}$. This illustrates that the accuracies of both spectral and the piecewise analytic representations converge roughly as $1/N_{\rm parms}$.

could be found. However, it is unlikely that such representations will be significantly more accurate than the representations studied here. Figure 15 shows that both the spectral and the piecewise analytic representations used here converge roughly as $1/N_{\rm parms}$. This $1/N_{\rm parms}$ convergence rate is the best that can be expected for piecewise analytic representations of discontinuous equations of state without any *a prior* knowledge of the locations or the sizes of the discontinuities. Given that the representations studied here already converge roughly at this rate, it is very unlikely that significantly better representations could be found.

### Acknowledgments

L.L. was supported in part by the National Science Foundation grants 2012857 and 2407545 to the University of California at San Diego, USA.

[1] L. Lindblom and N. M. Indik, Phys. Rev. D **86**, 084003 (2012).
[2] L. Lindblom and N. M. Indik, Phys. Rev. D **89**, 064003 (2014).
[3] L. Lindblom, AIP Conference Proceedings **1577**, 153 (2014).
[4] L. Lindblom, Phys. Rev. D **98**, 043012 (2018).
[5] F. Özel and P. Freire, Ann. Rev. Astron. and Astroph. **54**, 401 (2016).
[6] T. E. Riley et al., Astrophys. J. Lett. **887**, L21 (2019).
[7] M. C. Miller et al., Astrophys. J. Lett. **887**, L24 (2019).
[8] M. C. Miller et al., Astrophys. J. Lett. **918**, L28 (2021).
[9] B. Biswas, Astrophys. J. **921**, 63 (2021).
[10] S. Vinciguerra et al., Astrophys. J. **961**, 62 (2024).
[11] T. Salmi et al. (2024), arXiv:2406.14466.
[12] T. Choudhury et al., Astrophys. J. Lett. (2024), arXiv:2407.06789.
[13] K.Chatziioannou et al. (2024), arXiv:2407.11153.
[14] S. De, D. Finstad, J. M. Lattimer, D. A. Brown, E. Berger, and C. M. Biwer, Phys. Rev. Lett. **121**, 091102 (2018).
[15] S. De, D. Finstad, J. M. Lattimer, D. A. Brown, E. Berger, and C. M. Biwer, Phys. Rev. Lett. **121**, 259902 (2018).
[16] K. Chatziioannou, Gen. Relativ. Gravit. **52**, 109 (2020).
[17] J. S. Read, B. D. Lackey, B. J. Owen, and J. L. Friedman, Phys. Rev. **D79**, 124032 (2009).
[18] L. Lindblom, Phys. Rev. D **82**, 103011 (2010).
[19] L. Lindblom, Phys. Rev. D **97**, 123019 (2018).
[20] E. Annala, T. Gorda, A. Kurkela, J. Nattila, and A. Vourinen, Nature Physics **16**, 907 (2020).
[21] L. Lindblom, Phys. Rev. D **105**, 063031 (2022).
[22] L. Lindblom and T. Zhou, Phys. Rev. D **110**, 083030 (2024).
[23] L. Lindblom, Phys. Rev. D **110**, 043018 (2024).
[24] L. Lindblom and T. Zhou, Phys. Rev. D **111**, 063024 (2025).
[25] J. P. Boyd, *Chebyshev and Fourier Spectral Methods* (Dover Publications, 1999), 2nd ed.
[26] L. Lindblom, Phys. Rev. D **58**, 024008 (1998).
[27] V. Paschalidis, K. Yagi, D. Alvarez-Castillo, D. B. Blaschke, and A. Sedrakian, Phys. Rev. D **97**, 084038 (2018).
[28] P. L. Reed Essick and D. E. Holz, Phys. Rev. D **101**, 063007 (2020).
[29] D. Blaschke, D. E. Alvarez-Castillo, A. Ayriyan, H. Grigorian, N. K. Largani, and F. Weber, in *Topics on Strong Gravity: A Modern View on Theories and Experiments*, edited by C. A. Z. Vasconcellos (World Scientific, 2020), chap. 7, pp. 207–256.
[30] N. K. Glendenning, Phys. Rev. D **46**, 1274 (1992).
[31] N. K. Glendenning, Physics Reports **342**, 392 (2001).
[32] V. Abgaryan, D. Alvarez-Castillo, A. Ayriyan, D. Blaschke, and H. Grigorian, Universe **4**, 94 (2018).
[33] J. R. Oppenheimer and G. M. Volkoff, Phys. Rev. **55**, 374 (1939).
[34] L. D. Landau and E. M. Lifshitz, *Fluid Mechanics* (Pergamon Press, 1959).
[35] W. H. Press, S. A. Teukolsky, W. T. Vetterling, and B. P. Flannery, *Numerical Recipes in FORTRAN* (Cambridge University Press, Cambridge, England, 1992), 2nd ed.